Journal of Materials Chemistry

Cite this: J. Mater. Chem., 2012, 22, 11964

www.rsc.org/materials

PAPER

# Thermal stability of Fe–Mn binary olivine cathodes for Li rechargeable batteries†

Jongsoon Kim,[a] Kyu-Young Park,[a] Inchul Park,[a] Jung-Keun Yoo,[b] Jihyun Hong[a] and Kisuk Kang*[a]

*Received 7th February 2012, Accepted 8th April 2012*
**DOI: 10.1039/c2jm30733b**

The phase stability of binary Fe and Mn olivine materials is extensively studied with temperature-controlled *in situ* X-ray diffraction (XRD) for various Fe/Mn ratios and state of charges (SOCs). We identify that the thermal behavior of partially charged olivine materials is sensitively affected by the Fe/Mn ratio in the crystal. While Fe-rich binary olivine materials readily formed a solid solution phase of $Li_{1-y}Fe_{1-x}Mn_xPO_4$ near room temperature or with only slight heating, the Mn-rich binary olivine retained its two-phase characteristic up to *ca.* 250 °C before decomposition into non-olivine phases. The thermal stability and decomposition mechanism of fully delithiated olivine materials are more sensitively affected by the Fe/Mn ratio in the crystal. The decomposition temperature varies from 200 °C to 500 °C among the different Fe/Mn ratios. It is generally observed that the Mn-rich binary olivine materials are inferior to the Fe-rich ones with respect to the thermal stability in the delithiated state.



## 1. Introduction

Lithium transition metal phosphate $LiMPO_4$ (M = Mn, Fe, Co, and Ni) with an olivine structure is one of the most promising cathode candidates for lithium rechargeable batteries.[1–9] As the need for cost-effective, stable, and safe energy storage becomes unprecedentedly high due to the development of various types of electric vehicles and the large-scale energy storage systems for renewable energy sources, lithium rechargeable batteries based on $LiMPO_4$ cathodes have attracted much attention. In particular, naturally abundant Fe or Mn containing olivine $LiMPO_4$ has been most thoroughly investigated.[10–13] The stable nature of the olivine-type structure with a $(PO_4)^{3-}$ polyanion and a strong P–O covalent bond provides an excellent cycle-life in a safe manner. Moreover, a very high power capability has been demonstrated for the $LiFePO_4$ cathode material.[3,14–16] However, single component $LiFePO_4$ suffers from the intrinsic low energy density due to its relatively low $Fe^{2+}/Fe^{3+}$ redox potential (*ca.* 3.4 V *vs.* $Li^+/Li$).[4,6,17,18] On the other hand, $LiMnPO_4$ can theoretically deliver a higher energy density due to the high redox potential of $Mn^{2+}/Mn^{3+}$ (*ca.* 4.1 V *vs.* $Li^+/Li$), while its power capability is significantly reduced. To counterbalance such an effect, binary $LiFe_{1-x}Mn_xPO_4$ olivine cathodes have been explored by researchers.[10,11,14] Recent works have shown that the electrochemical properties of binary $LiFe_{1-x}Mn_xPO_4$ cathodes are sensitively dependent on the Fe/Mn ratio in the material.[10–13] Power capability, energy density, and even the charge/discharge mechanism (one-phase *vs.* two-phase) vary with different Fe/Mn ratios clearly indicating that the optimal composition of Fe/Mn in the binary $LiFe_{1-x}Mn_xPO_4$ needs to be determined.[2,10,19–21]

In the present work, the phase stability of binary $LiFe_{1-x}Mn_xPO_4$ ($x = 0$, 0.25, 0.5, 0.75, and 1) was investigated with different Li compositions and temperatures with temperature-controlled *in situ* XRD. Since the safety and stability of the battery is strongly influenced by the phase stability of the cathode at different SOCs and temperatures, this work can provide useful information in determining the optimal composition of binary $LiFe_{1-x}Mn_xPO_4$ cathodes. Earlier work on the thermal stability of single component $LiFePO_4$ and $LiMnPO_4$ with experiments and DFT calculation[22–25] showed that both $LiFePO_4$ and $LiMnPO_4$ remain stable up to fairly high temperatures; however, partially or fully delithiated $Li_xMnPO_4$ decomposes at *ca.* 200 °C with $O_2$ evolution and heat generation in the process, while delithiated $FePO_4$ is stable until *ca.* 500 °C.[22–24] In this study, we were able to confirm the higher stability of $FePO_4$ compared to $MnPO_4$, and further demonstrate the difference in the relative stabilities of the phases in delithiated $LiFe_{1-x}Mn_xPO_4$ with comparative analyses of the *in situ* XRD patterns using different Fe/Mn ratios in $LiFe_{1-x}Mn_xPO_4$.

## 2. Experimental

$LiFe_{1-x}Mn_xPO_4$ powder was synthesized using the conventional solid-state synthesis. $Li_2CO_3$ (Junsei Chemical, 98%), $Mn(CH_3COO)_2 \cdot 4H_2O$ (Junsei Chemical, 98%), $FeC_2O_4 \cdot 2H_2O$

[a]Department of Materials Science and Engineering, Seoul National University, 599 Gwanak-ro, Gwanak-gu, Seoul, Korea 151-742. E-mail: matlgen1@snu.ac.kr; Fax: +82-2-885-9671; Tel: +82-2-880-7088
[b]Department of Materials Science and Engineering, KAIST (Korea Advanced Institute of Science and Technology), Gwahangno 335, Yuseong-gu, Daejeon, Korea 305-701

† Electronic supplementary information (ESI) available: The phase purity and reference thermal behavior of as-prepared $LiFe_{1-x}Mn_xPO_4$ and the phase purity of the delithiated $Li_{1-y}Fe_{1-x}Mn_xPO_4$ samples. See DOI: 10.1039/c2jm30733b

(Sigma Aldrich, 98%), and $NH_4H_2PO_4$ (Fluka, 98%) with molar ratios of $0.5 : x : 1 - x : 1$ ($x = 0$, 0.25, 0.5, 0.75, and 1) were used as precursors. They were dispersed into acetone, thoroughly mixed, and ground by wet ball-milling. After evaporating the acetone, the precursors were then fired at 350 °C under Ar conditions for 3 hours. The mixture was then re-ground and manually pelletized using a disk-shaped mold. After pre-heating, we calcined the pellets at 600 °C under Ar conditions for 10 hours.

To prepare the $Li_{1-y}Fe_{1-x}Mn_xPO_4$ samples, the synthesized $LiFe_{1-x}Mn_xPO_4$ was chemically delithiated by $NO_2BF_4$ (Aldrich, 95%) according to the following reaction.

$$LiFe_{1-x}Mn_xPO_4 + yNO_2BF_4 \rightarrow Li_{1-y}Fe_{1-x}Mn_xPO_4 + yLiBF_4 + yNO_2$$

$NO_2BF_4$ is a strong oxidizing agent with a high redox potential of $NO_2^+/NO_2$ at 5.1 V *vs.* $Li^+/Li$. The composition of $Li_{1-y}Fe_{1-x}Mn_xPO_4$ was controlled by governing the time of the reaction between the $LiFe_{1-x}Mn_xPO_4$ and $NO_2BF_4$ with a molar ratio of 1 : 1 in acetonitrile (Aldrich, 98%) in an Ar-filled glove box. The stoichiometry of the delithiated compound was determined by inductively coupled plasma-atomic emission spectroscopy (ICP-AES). The atomic ratios of Li, Fe, and Mn in as-prepared, partially delithiated, and fully delithiated $Li_{1-y}Fe_{1-x}Mn_xPO_4$ ($x = 0$, 0.25, 0.5, 0.75, and 1; $0 \leq y \leq 1$) are summarized in Table S1†. The crystal structure was determined by XRD (Rigaku D/Max 2500) with Cu K$\alpha$ radiation (= 1.54178 Å) operating at 30 kV and 400 mA. For the temperature-dependent phase stability study, samples were heated from 25 °C to 700 °C in a vacuum during the XRD investigation. The heating rate was 5 °C $min^{-1}$; the waiting time between heating and measurement was 3 min, and the scan speed was 1° $min^{-1}$. Structural refinements were done by the Rietveld method with a general structure analysis system (GSAS).

## 3. Computational details

The hypothetical $(Fe_{1-x}Mn_x)_3(PO_4)_2$ and $(Fe_{1-x}Mn_x)_2P_2O_7$ ($x =$ 0.25, 0.5, and 0.75) structures were calculated from the first principles, starting from the $Fe_3(PO_4)_2$ and $Fe_2P_2O_7$ structures.[26] Calculations were done on the entire Fe/Mn ordered configurations to find the most stable structure of the solid solution. The spin-polarized generalized gradient approximation (GGA) was applied with the Perdew–Burke–Ernzerhof exchange-correlation parameterization[27] for the density functional theory (DFT). A plane-wave basis set and the projector-augmented wave (PAW) method were used as implemented in the Vienna *ab initio* simulation package (VASP).[28] PAW potentials have been widely used for battery materials and have shown good predictive capability.[29–32] Plane-wave bases with a kinetic energy cutoff of 500 eV were used, and appropriate *k*-point meshes were chosen to ensure that the total energy converged within 5 meV per formula unit.

## 4. Results and discussion

The phase purity and reference thermal behavior of as-prepared $LiFe_{1-x}Mn_xPO_4$ were first checked, as shown in Fig. S1–S3† and Tables S2 and S3†. Also, the phase purity of the delithiated $Li_{1-y}Fe_{1-x}Mn_xPO_4$ samples is confirmed in Fig. S4†. The obtained samples are used in the following thermal phase stability studies.

### 4.1 Revisit of $Li_{1-y}FePO_4$ and $Li_{1-y}MnPO_4$ ($0 < y \leq 1$)

While the $FePO_4$ phase retained its original XRD pattern from 25 °C to 450 °C (Fig. S5(a)†) in agreement with a previous report,[22] it started to decompose into a new phase at 500 °C. As shown in Fig. 1(a), a new phase with main peaks located at 25°, 29°, 31°, and 35° arose at 500 °C, which correspond to the typical XRD pattern of $Fe_3(PO_4)_2$. The XRD peaks for $Fe_3(PO_4)_2$ significantly reduced at 600 °C, and those of $Fe_2P_2O_7$ started to appear and grow at this temperature. Especially, the growth of a new phase was remarkably clear at *ca.* 29°, which is the main XRD peak of $Fe_2P_2O_7$. This observation agrees with the analysis of thermal stability of $FePO_4$ by Ong *et al.* that predicted a three-step decomposition using DFT calculations: $FePO_4 \rightarrow 0.1(Fe_7(PO_4)_6 + Fe_3(P_2O_7)_2) \rightarrow 0.167(Fe_3(PO_4)_2 + Fe_3(P_2O_7)_2) \rightarrow 0.5Fe_2P_2O_7$.[25] Although we did not observe the first step of the decomposition they predicted, the second and the final steps of the decomposition indicated the sequential formation of $Fe_3(PO_4)_2$ and $Fe_2P_2O_7$ consistent with our experimental observation. Nevertheless, we could not determine the $Fe_3(P_2O_7)_2$ phase with certainty. The decomposition of $FePO_4$ into $Fe_3(PO_4)_2$ would result in an imbalance of the Fe : P stoichiometry. Thus, another new P-rich phase had to be formed. However, it was not possible to clearly define a new P-rich phase indicating that amorphorization had occurred to some extent at the phase transition. It should be noted that compositions with high phosphorus content are known to be very good glass formers.[33]

In the case of partially delithiated $Li_{0.6}FePO_4$, a two-phase reaction of $LiFePO_4$ and $FePO_4$ is clearly confirmed from 25 °C to 350 °C in Fig. S6(a)†. When the temperature was elevated to *ca.* 400 °C, the XRD patterns of both $LiFePO_4$ and $FePO_4$ started to merge with the appearance of broad patterns for the solid solution phase as highlighted with the circle in Fig. 1(b).[22] At the temperatures higher than *ca.* 600 °C, the solid solution $Li_{0.6}FePO_4$ phase began to decompose into $Fe_2P_2O_7$, as shown in Fig. 1(c). The emergence of XRD peaks of $Fe_2P_2O_7$ becomes clear at or above 600 °C. In addition, it should be noted that the solid solution $Li_{0.6}FePO_4$ pattern was very similar to that of $LiFePO_4$ from 600 °C. The change in XRD patterns from solid solution to fully lithiated $LiFePO_4$ was easily observed at the $2\theta$ range between 37° and 40°. The comparison of the lattice parameter as a function of temperature in Fig. S7(a)† clearly demonstrates the formation of $LiFePO_4$ from the $Li_{0.6}FePO_4$ solid solution between 550 °C and 600 °C. Previously, Delacourt *et al.* reported that the partially delithiated $Li_{1-y}FePO_4$ decomposes into $Fe_7(PO_4)_6$.[22] However, except for the XRD peaks of *ca.* 29° and 35°, most of the XRD peaks of $Fe_7(PO_4)_6$ did not correspond to those of the new non-olivine phase. Instead, we observed that these new XRD peaks were similar to those of decomposition products of fully delithiated $FePO_4$ at 700 °C, which is equivalent to $Fe_2P_2O_7$, as shown in Fig. S7(b)†. It means that the solid solution $Li_{0.6}FePO_4$ decomposes into $Fe_2P_2O_7$ leaving the fully lithiated olivine phase ($LiFePO_4$) behind.

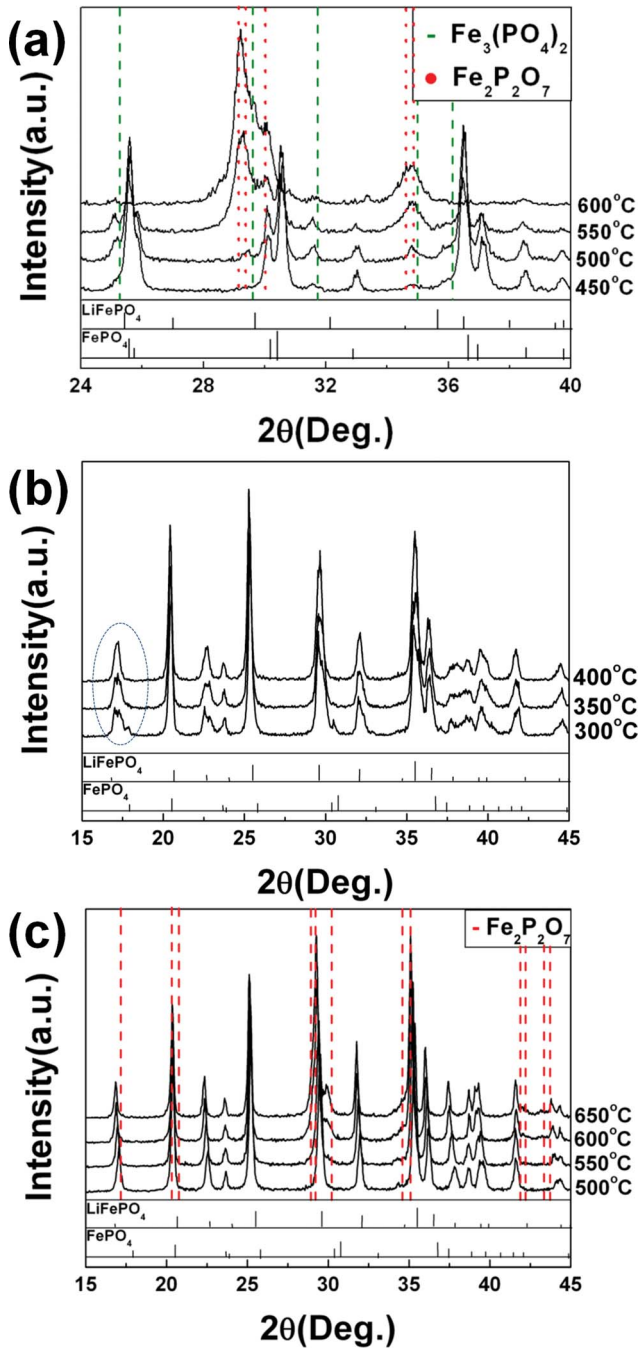


**Fig. 1** (a) *In situ* XRD patterns of fully delithiated $FePO_4$ at temperatures from 450 °C to 600 °C and at $2\theta$ from 24° to 40°, (b) *in situ* XRD patterns of partially delithiated $Li_{0.6}FePO_4$ at temperatures from 300 °C to 400 °C and at $2\theta$ from 15° to 45°, and (c) *in situ* XRD patterns of partially delithiated $Li_{0.6}FePO_4$ at temperatures from 500 °C to 650 °C and at $2\theta$ from 15° to 45°.

$MnPO_4$ exhibited a similar thermal decomposition mechanism to $FePO_4$. At low temperatures from 25 °C to 200 °C, no noticeable phase transition of $MnPO_4$ was observed (Fig. S5(b)†). However, at temperatures above 200 °C, the $MnPO_4$ phase decomposed into a new non-olivine phase. At the temperature range from 200 °C to 400 °C, $Mn_3(PO_4)_2$ (main peak at *ca.* 25°) was formed and it is consistent with our previous report.[34] Similar to the decomposition of $FePO_4$ into $Fe_3(PO_4)_2$, the decomposition of $MnPO_4$ into $Mn_3(PO_4)_2$ would also result in an imbalance of the Mn : P stoichiometry. We expect that an amorphous P-rich phase that is not detectable by XRD would have formed during the decomposition to compensate for the imbalance of composition. A further increase of the temperature completely amorphorized the sample at 550 °C followed by the formation of $Mn_2P_2O_7$ at 600 °C, as shown in Fig. S8†.

The phase transition of partially delithiated $Li_{0.5}MnPO_4$ occurred at a similar temperature range, from 250 °C, as shown in Fig. 2(a) (full temperature scan of $Li_{0.5}MnPO_4$ is provided in Fig. S6(b)†). Instead of forming the solid solution of $Li_{0.5}MnPO_4$ at high temperature, the fully delithiated phase $MnPO_4$ gradually disappeared and the $Mn_3(PO_4)_2$ phase started to appear. The formation of $Mn_3(PO_4)_2$ is consistent with the decomposition case of the fully delithiated $MnPO_4$ sample. At 550 °C, $Mn_2P_2O_7$ was finally formed from $Mn_3(PO_4)_2$ as shown in Fig. 2(b).

### 4.2 Phase stability of an Fe–Mn binary olivine at elevated temperatures

**4.2.1 $Li_{1-y}Fe_{0.75}Mn_{0.25}PO_4$ ($0 < y \leq 1$).** Fully delithiated $Fe_{0.75}Mn_{0.25}PO_4$ began to decompose into new non-olivine phases from 500 °C (full temperature scan of $Fe_{0.75}Mn_{0.25}PO_4$ is provided in Fig. S5(c)†). As shown in Fig. 3(a), the peaks at *ca.* 25°, 29°, 31°, and 35° became embossed at 500 °C. These peaks corresponded to the general XRD patterns of $M_3(PO_4)_2$ (M = Fe or Mn). At this point, it is not clear if $Fe_{0.75}Mn_{0.25}PO_4$ decomposed into a mixture of $Fe_3(PO_4)_2$ and $Mn_3(PO_4)_2$ or a solid solution $(Fe_{0.75}Mn_{0.25})_3(PO_4)_2$. It appears that the observed XRD peaks do not exactly match with either $Fe_3(PO_4)_2$ or $Mn_3(PO_4)_2$, but lie between those two patterns. This strongly implies that a solid solution, $(Fe_{0.75}Mn_{0.25})_3(PO_4)_2$, had formed. In order to confirm it, we did a DFT (Density Functional Theory) calculation on the $(Fe_{0.75}Mn_{0.25})_3(PO_4)_2$ to predict its crystal structure and generated an XRD pattern from the structure. The dotted line in Fig. 3(a) is the XRD pattern for the hypothetical $(Fe_{0.75}Mn_{0.25})_3(PO_4)_2$, which perfectly agrees with the observation. Therefore, we supposed that $Fe_{0.75}Mn_{0.25}PO_4$ decomposed into $(Fe_{0.75}Mn_{0.25})_3(PO_4)_2$. As in the case of $FePO_4$ and $MnPO_4$, the decomposition of $Fe_{0.75}Mn_{0.25}PO_4$ into $(Fe_{0.75}Mn_{0.25})_3(PO_4)_2$ resulted in an imbalance of the (Fe, Mn) : P stoichiometry. Thus, the formation of an amorphous P-rich phase is expected.

With a further increase of the temperature, new peaks at *ca.* 29° and 35°, characteristic of the $M_2P_2O_7$ (M = Fe or Mn) XRD pattern, dominantly grew with the disappearance of $(Fe_{0.75}Mn_{0.25})_3(PO_4)_2$ at 550 °C. This behavior is analogous to the decomposition mechanism of $Fe_3(PO_4)_2$ to $Fe_2P_2O_7$ for $FePO_4$ and $Mn_3(PO_4)_2$ to $Mn_2P_2O_7$ for $MnPO_4$. The observed XRD peaks also did not exactly match with either $Fe_2P_2O_7$ or $Mn_2P_2O_7$. Instead, the calculated XRD pattern from the hypothetical $(Fe_{0.75}Mn_{0.25})_2P_2O_7$ from the DFT calculation perfectly agreed with the observed XRD pattern (dashed line in Fig. 3(a)).

Unlike the aforementioned single component olivine materials (= $LiFePO_4$ and $LiMnPO_4$), the partial delithiation ($Li \approx 0.44$) of $LiFe_{0.75}Mn_{0.25}PO_4$ resulted in a single phase at 25 °C.[19] Heating of this sample until 500 °C did not induce any noticeable phase transformation demonstrating its high thermal stability

 

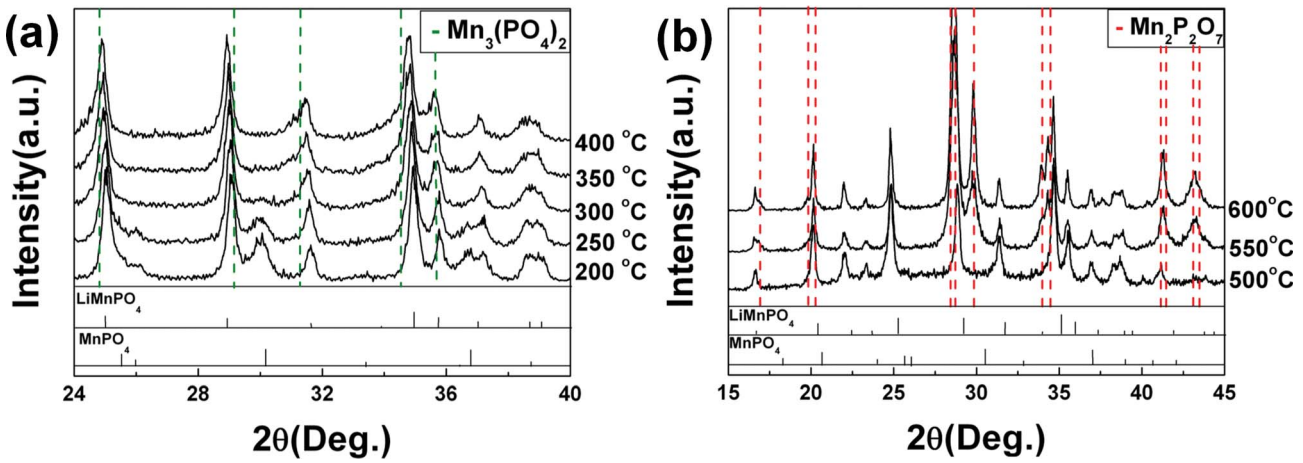


**Fig. 2** (a) *In situ* XRD patterns of partially delithiated $Li_{0.5}MnPO_4$ at temperatures from 200 °C to 400 °C, and at $2\theta$ from 24° to 40° and (b) *in situ* XRD patterns of partially delithiated $Li_{0.5}MnPO_4$ at temperatures from 500 °C to 600 °C and at $2\theta$ from 15° to 45°.

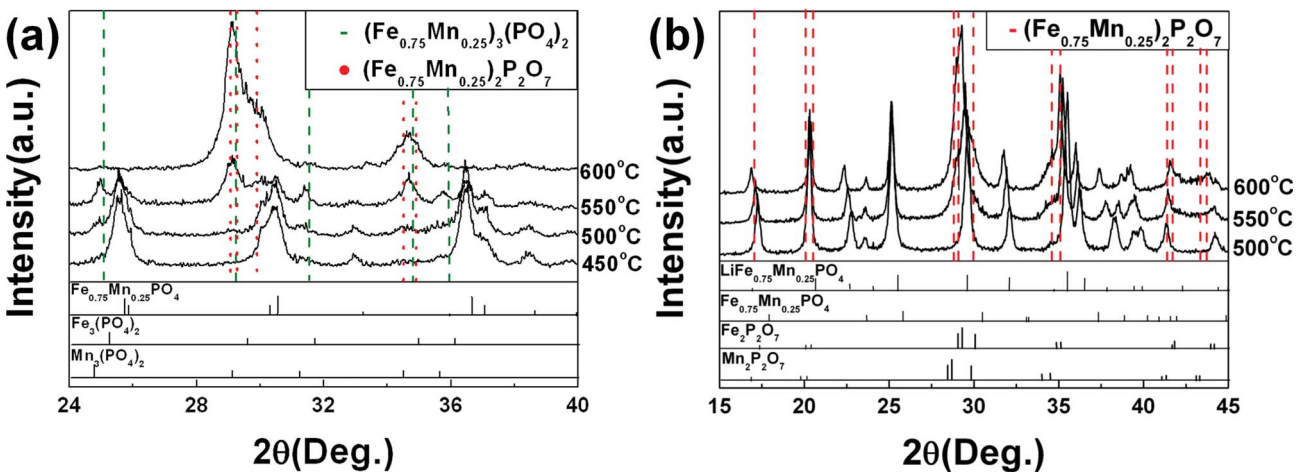


**Fig. 3** (a) *In situ* XRD patterns of fully delithiated $Fe_{0.75}Mn_{0.25}PO_4$ at temperatures from 450 °C to 550 °C and at $2\theta$ from 24° to 40° and (b) *in situ* XRD patterns of partially delithiated $Li_{0.44}Fe_{0.75}Mn_{0.25}PO_4$ at temperatures from 500 °C to 600 °C at $2\theta$ from 15° to 45°.

(Fig. S6(c)†). Only the thermal expansion of the olivine crystal $Li_{0.44}Fe_{0.75}Mn_{0.25}PO_4$ was observed as indicated by the shift of the XRD peaks at elevated temperatures. However, Fig. 3(b) shows that the single phase $Li_{0.44}Fe_{0.75}Mn_{0.25}PO_4$ decomposed into fully lithiated olivine $LiFe_{0.75}Mn_{0.25}PO_4$ and non-olivine phases at 550 °C analogous to the behavior of the partially delithiated $Li_{1-y}FePO_4$. The growth of the XRD peaks at *ca.* 29° and 35° began at 550 °C, which indicates the formation of the $M_2P_2O_7$ (M = Fe, Mn) phase. Simultaneously, all XRD peaks of solid solution $Li_{0.44}Fe_{0.75}Mn_{0.25}PO_4$ were shifted toward those of the fully lithiated $LiFe_{0.75}Mn_{0.25}PO_4$ (Fig. S9(a)†). The thermal decomposition at 550 °C resulted in $M_2P_2O_7$ (M = Fe, Mn) with its XRD peaks different from either $Fe_2P_2O_7$ or $Mn_2P_2O_7$. These XRD peaks corresponded to the $(Fe_{0.75}Mn_{0.25})_2P_2O_7$ structure that we predicted from the DFT calculation.

**4.2.2 $Li_{1-y}Fe_{0.5}Mn_{0.5}PO_4$ ($0 < y \leq 1$).** The overall decomposition mechanism of $Fe_{0.5}Mn_{0.5}PO_4$ appeared to be similar to that of $Fe_{0.75}Mn_{0.25}PO_4$ except the relatively lower decomposition temperature of 350 °C. Fig. 4(a) shows that $Fe_{0.5}Mn_{0.5}PO_4$ starts to decompose into $(Fe_{0.5}Mn_{0.5})_3(PO_4)_2$ at 350 °C. The emerging peaks in the XRD pattern at this temperature corresponded with the hypothetical $(Fe_{0.5}Mn_{0.5})_3(PO_4)_2$ structure from the DFT calculation. When the temperature rose to 550 °C, new XRD peaks such as at *ca.* 29° and 35° started to grow. We also found that they were close to the calculated XRD peaks of the hypothetical $(Fe_{0.5}Mn_{0.5})_2P_2O_7$ structure predicted from the DFT calculation, as shown in Fig. 4(b). Thereafter, the $(Fe_{0.5}Mn_{0.5})_2P_2O_7$ phase grew at the expense of $Fe_{0.5}Mn_{0.5}PO_4$ and $(Fe_{0.5}Mn_{0.5})_3(PO_4)_2$. It should be noted that slightly higher Mn contents (25% *vs.* 50%) in binary olivine materials significantly decrease the decomposition temperature of the delithiated phase from 500 °C to 350 °C.

Dissimilar to the partially delithiated $Li_{0.44}Fe_{0.75}Mn_{0.25}PO_4$, which was in a single phase at room temperature, the partially delithiated $Li_{0.4}Fe_{0.5}Mn_{0.5}PO_4$ exhibited the mixed behavior of one-phase and two-phase (Fig. S6(d)†). However, with a slight increase in the temperature, the residual two phases merged into a single phase as highlighted with a circle in Fig. 4(c). Once the solid solution phase of $Li_{0.4}Fe_{0.5}Mn_{0.5}PO_4$ was formed, its

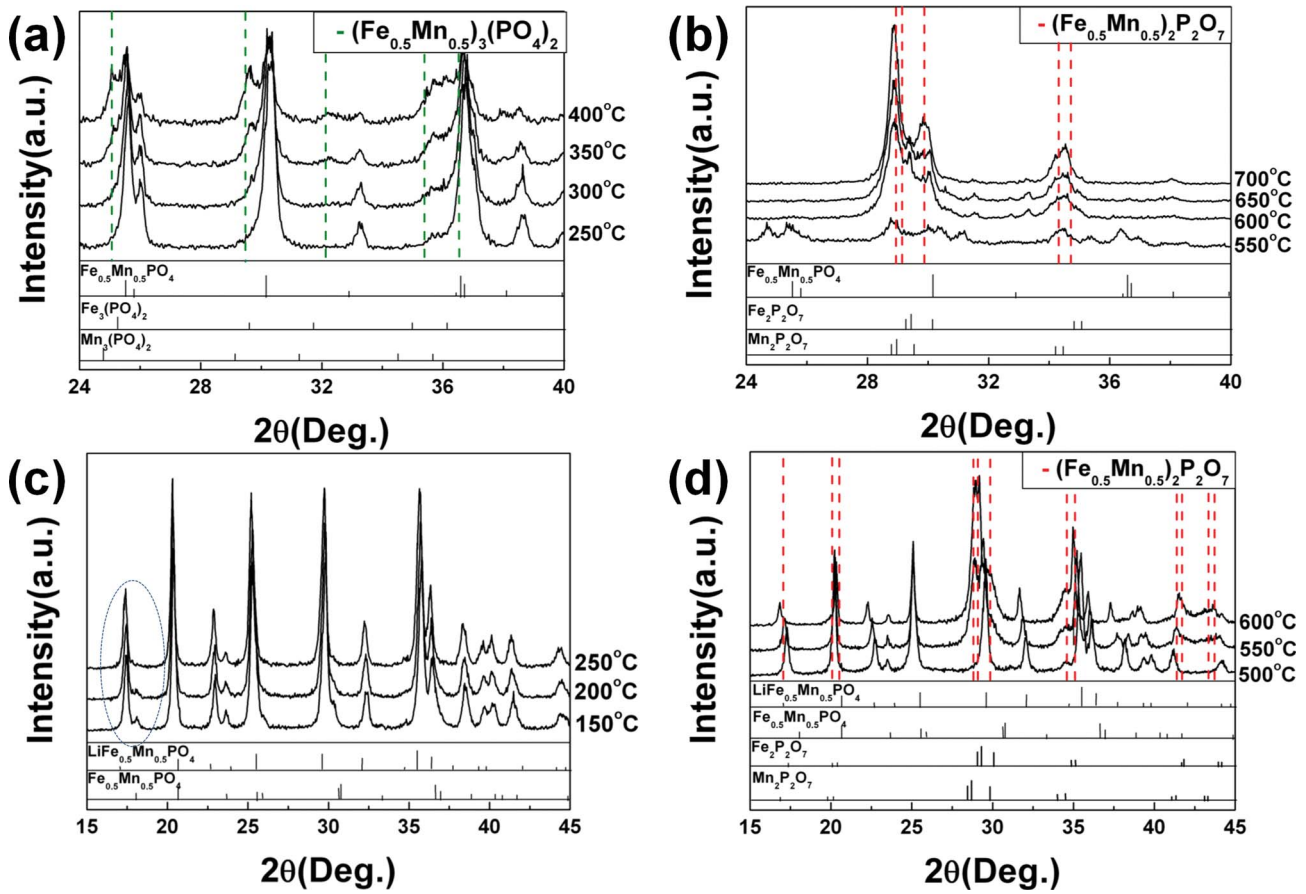


**Fig. 4** (a) *In situ* XRD patterns of fully delithiated $Fe_{0.5}Mn_{0.5}PO_4$ at temperatures from 250 °C to 400 °C and at $2\theta$ from 24° to 40°, (b) *in situ* XRD patterns of fully delithiated $Fe_{0.5}Mn_{0.5}PO_4$ at temperatures from 550 °C to 700 °C and at $2\theta$ from 24° to 40°, (c) *in situ* XRD patterns of partially delithiated $Li_{0.4}Fe_{0.5}Mn_{0.5}PO_4$ at temperatures from 150 °C to 250 °C and at $2\theta$ from 15° to 45°, and (d) *in situ* XRD patterns of partially delithiated $Li_{0.4}Fe_{0.5}Mn_{0.5}PO_4$ at temperatures from 500 °C to 600 °C and at $2\theta$ from 15° to 45°.

decomposition path became analogous to that of $Li_{0.44}Fe_{0.75}Mn_{0.25}PO_4$, where the mixture of the fully lithiated olivine phase (= $LiFe_{0.5}Mn_{0.5}PO_4$) and $(Fe_{0.5}Mn_{0.5})_2P_2O_7$ appeared at 550 °C (Fig. 4(d) and S9(b)†).

**4.2.3 $Li_{1-y}Fe_{0.25}Mn_{0.75}PO_4$ ($0 < y \leq 1$).** From 25 °C to 250 °C, noticeable changes in the XRD pattern of $Fe_{0.25}Mn_{0.75}PO_4$ were not observed similar to the other delithiated $Fe_{1-x}Mn_xPO_4$ samples (Fig. S5(e)†). However, upon heating higher than 300 °C, new XRD peaks appeared. As shown in Fig. 5(a), $Fe_{0.25}Mn_{0.75}PO_4$ decomposed into $(Fe_{0.25}Mn_{0.75})_3(PO_4)_2$ whose structure was calculated from the DFT calculation. This behavior was consistent with the other $Fe_{1-x}Mn_xPO_4$. However, it should be noted that the decomposition temperature significantly decreased from 550 °C to 300 °C. This strongly suggests the disadvantage of high Mn content binary olivine materials in terms of phase stability. In addition, it should be emphasized that the Mn effect on inferior thermal stability began to be observed when Mn ≥ 50% for partially delithiated binary olivine materials, but for the fully delithiated phase, the effect was observed for higher contents of Mn (Mn ≥ 75%). Upon further heating higher than 550 °C, $(Fe_{0.25}Mn_{0.75})_2P_2O_7$ was formed, as shown in Fig. 5(b).

As in the case of $Li_{0.46}Fe_{0.25}Mn_{0.75}PO_4$, the two-phase mixture was converted to a solid solution of $Li_{0.46}Fe_{0.25}Mn_{0.75}PO_4$ with a slight increase in temperature shown in Fig. 5(c). However, the phase transition temperature of $Li_{0.46}Fe_{0.25}Mn_{0.75}PO_4$ increased from 250 °C to 300 °C, compared to that of $Li_{0.4}Fe_{0.5}Mn_{0.5}PO_4$. It indicates that the higher Mn content binary olivine prefers a two-phase separation more strongly. This is mainly due to a stronger lattice distortion induced by Jahn–Teller active $Mn^{3+}$ in the Mn-rich olivine materials. When the lattice mismatch becomes significantly bigger, the elastic strain cannot be stored by the lattice distortion and the precipitates tend to be separated from the mother phase.[35,36] Once the solid solution phase of $Li_{0.46}Fe_{0.25}Mn_{0.75}PO_4$ was formed, its decomposition path became analogous to that of $Li_{0.44}Fe_{0.75}Mn_{0.25}PO_4$ and $Li_{0.4}Fe_{0.5}Mn_{0.5}PO_4$, where the mixture of the fully lithiated olivine phase ($Li_{0.44}Fe_{0.25}Mn_{0.75}PO_4$) and $(Fe_{0.25}Mn_{0.75})_2P_2O_7$ appeared at 550 °C (Fig. 5(d) and S9(c)†).

### 4.3 Phase stability map of an Fe–Mn binary olivine as a function of temperature and Li amount in the structure

From the extensive series of XRD results above, it was found that the $Li_{1-y}Fe_{1-x}Mn_xPO_4$ ($0 \leq x, y \leq 1$) displayed different

 

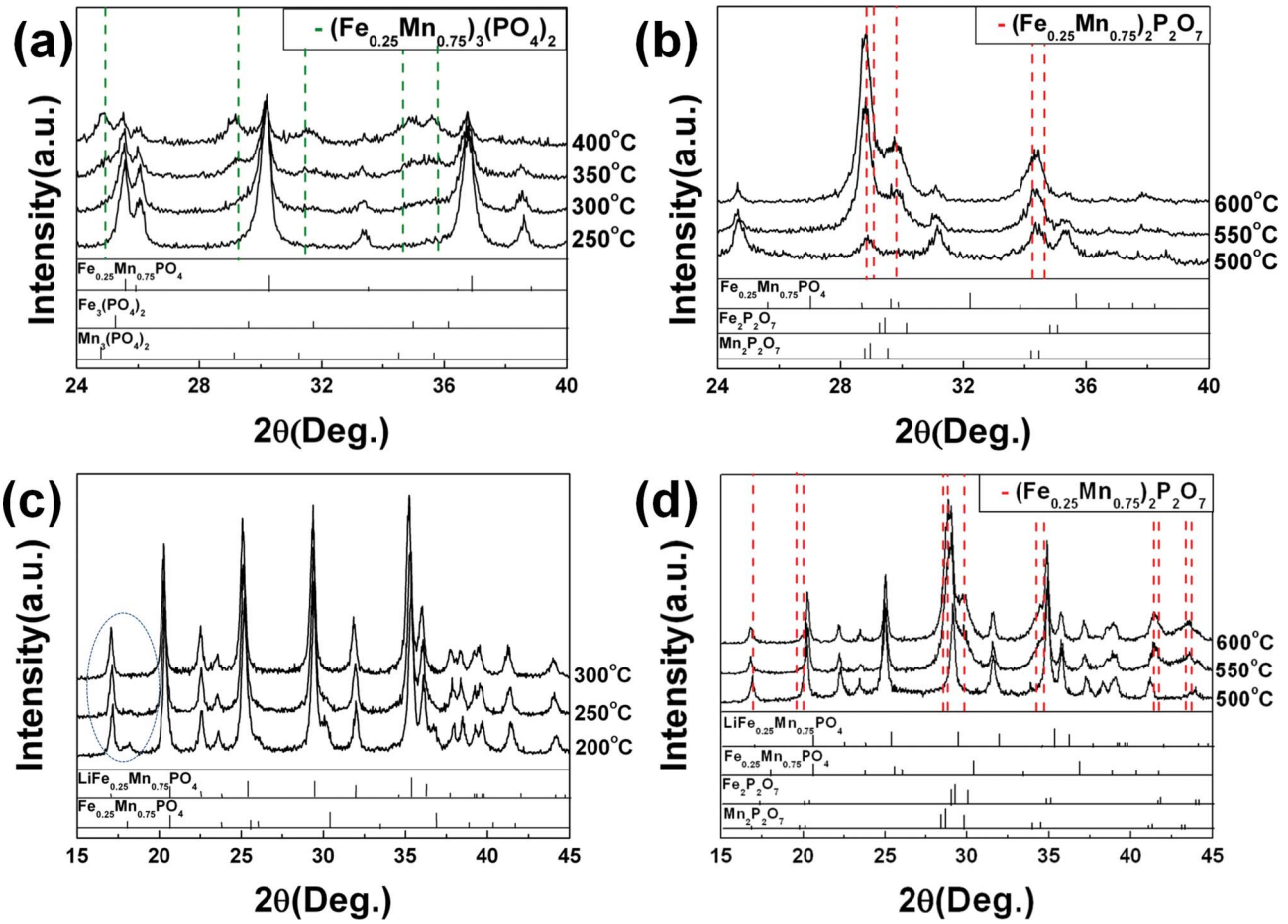


**Fig. 5** (a) *In situ* XRD patterns of fully delithiated $Fe_{0.25}Mn_{0.75}PO_4$ at temperatures from 250 °C to 400 °C and at $2\theta$ from 24° to 40°, (b) *in situ* XRD patterns of fully delithiated $Fe_{0.25}Mn_{0.75}PO_4$ at temperatures from 500 °C to 600 °C and at $2\theta$ from 24° to 40°, (c) *in situ* XRD patterns of partially delithiated $Li_{0.46}Fe_{0.25}Mn_{0.75}PO_4$ at temperatures from 200 °C to 300 °C and at $2\theta$ from 15° to 45°, and (d) *in situ* XRD patterns of partially delithiated $Li_{0.46}Fe_{0.25}Mn_{0.75}PO_4$ at temperatures from 500 °C to 600 °C and at $2\theta$ from 15° to 45°.

thermal characteristics depending on the Fe/Mn and Li contents in the olivine structures. A summary of the stable phases of $Li_{1-y}Fe_{1-x}Mn_xPO_4$ ($0 \leq x \leq 1$) upon heating is shown in Fig. 6 and 7 with respect to the Li and Fe/Mn contents. While the fully lithiated $LiFe_{1-x}Mn_xPO_4$ ($0 \leq x \leq 1$) phases were highly stable at high temperature, it was observed that delithiated phases were susceptible to partial phase transformation upon heating. In the phase stability map of fully delithiated phases of $Fe_{1-x}Mn_xPO_4$ ($0 \leq x \leq 1$) in Fig. 6, we observed that the thermal decomposition temperature generally declined with an increase in the Mn content in the olivine structure. A significant drop in the decomposition temperature was observed when the Mn content exceeded the Fe content in the olivine. In the phase stability map of partially delithiated phases of $Li_{1-y}Fe_{1-x}Mn_xPO_4$ ($0 \leq x \leq 1$, $y \approx 0.6$) in Fig. 7, the two-phase characteristic of $(1 - y)$ $LiFe_{1-x}Mn_xPO_4$ + $yFe_{1-x}Mn_xPO_4$ disappeared upon a slight increase in the temperature. In the case of Fe-rich binary olivine materials, a solid solution behavior was observed even at room temperature, while a higher Mn content in binary olivine materials exhibited a stronger two-phase preference. Contrary to the sensitivity of solid solution formation depending on the Fe/Mn content, the decomposition temperature into $(Fe_{1-x}Mn_x)_2P_2O_7$ was similar among samples. Notable is the fact that Fe-rich binary olivine materials exhibit a wider temperature window for the solid solution phase before decomposing into $(Fe_{1-x}Mn_x)_2P_2O_7$.

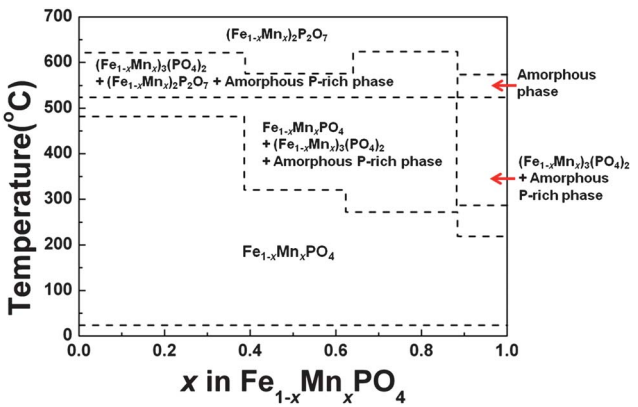


**Fig. 6** The phase stability map of fully delithiated $Fe_{1-x}Mn_xPO_4$ ($0 \leq x \leq 1$) as functions of temperature.

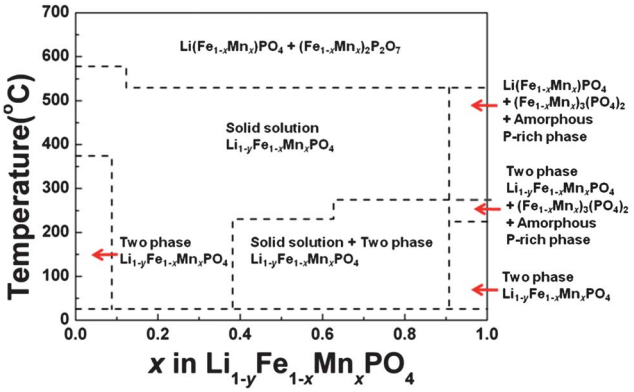


**Fig. 7** The phase stability map of partially delithiated $Li_{1-y}Fe_{1-x}Mn_xPO_4$ ($0 \leq x \leq 1$, $y \approx 0.6$) as functions of temperature.

## 5. Conclusion

In summary, the phase stability of $Li_{1-y}Fe_{1-x}Mn_xPO_4$ ($0 \leq x, y \leq 1$) during delithiation and lithiation was investigated as a function of the temperature, the Li composition, and the Fe or Mn amounts in the structure with temperature-controlled *in situ* XRD. Fully lithiated $LiFe_{1-x}Mn_xPO_4$ ($0 \leq x \leq 1$) remained stable up to high temperatures (>700 °C). However, the thermal stability of delithiated $Li_{1-y}Fe_{1-x}Mn_xPO_4$ ($0 \leq x, y \leq 1$) was influenced sensitively by the Fe/Mn content in the structure. Furthermore, the delithiation mechanism (one-phase *vs.* two-phase reaction) was dependent on the Fe/Mn ratio. It was generally observed that higher Mn content binary olivine materials exhibited inferior thermal stabilities in the charged states and a stronger preference for the two-phase behavior.

## Acknowledgements

This work was supported by Energy Efficiency and Resources R&D program (20112020100070) under the Ministry of Knowledge Economy, Republic of Korea, and by Human Resources Development of the Korea Institute of Energy Technology Evaluation and Planning (KETEP) grant funded by the Korea government Ministry of Knowledge Economy (20114010203120) and a grant from the Fundamental R&D Program for Technology of World Premier Materials funded by the Ministry of Knowledge Economy, Republic of Korea, and KISTI supercomputing center through the strategic support program for the supercomputing application research (No. KSC-2010-C2-0006).

## Notes and references

1 A. K. Padhi, K. S. Nanjundaswamy and J. B. Goodenough, *J. Electrochem. Soc.*, 1997, **144**, 1188–1194.
2 A. Yamada, Y. Takei, H. Koizumi, N. Sonoyama, R. Kanno, K. Itoh, M. Yonemura and T. Kamiyama, *Chem. Mater.*, 2006, **18**, 804–813.
3 S. Y. Chung, J. T. Bloking and Y. M. Chiang, *Nat. Mater.*, 2002, **1**, 123–128.
4 J. Kim, Y. U. Park, D. H. Seo, J. Kim, S. W. Kim and K. Kang, *J. Electrochem. Soc.*, 2011, **158**, A250–A254.
5 H. Gwon, D. H. Seo, S. W. Kim, J. Kim and K. Kang, *Adv. Funct. Mater.*, 2009, **19**, 3285–3292.
6 J. Kim, D. H. Seo, S. W. Kim, Y. U. Park and K. Kang, *Chem. Commun.*, 2010, **46**, 1305–1307.
7 Y.-U. Park, J. Kim, H. Gwon, D. H. Seo, S. W. Kim and K. Kang, *Chem. Mater.*, 2010, **22**, 2573.
8 D. Rangappa, K. Sone, Y. Zhou, T. Kudo and I. Honma, *J. Mater. Chem.*, 2011, **21**, 15813–15818.
9 G. Y. Chen, A. K. Shukla, X. Y. Song and T. J. Richardson, *J. Mater. Chem.*, 2011, **21**, 10126–10133.
10 A. Yamada, Y. Kudo and K. Y. Liu, *J. Electrochem. Soc.*, 2001, **148**, A747–A754.
11 K. Saravanan, J. J. Vittal, M. V. Reddy, B. V. R. Chowdari and P. Balaya, *J. Solid State Electrochem.*, 2010, **14**, 1755–1760.
12 S. M. Oh, H. G. Jung, C. S. Yoon, S. T. Myung, Z. H. Chen, K. Amine and Y. K. Sun, *J. Power Sources*, 2011, **196**, 6924–6928.
13 B. Zhang, X. J. Wang, H. Li and X. J. Huang, *J. Power Sources*, 2011, **196**, 6992–6996.
14 M. Yonemura, A. Yamada, Y. Takei, N. Sonoyama and R. Kanno, *J. Electrochem. Soc.*, 2004, **151**, A1352–A1356.
15 P. S. Herle, B. Ellis, N. Coombs and L. F. Nazar, *Nat. Mater.*, 2004, **3**, 147–152.
16 Y. G. Wang, Y. R. Wang, E. J. Hosono, K. X. Wang and H. S. Zhou, *Angew. Chem., Int. Ed.*, 2008, **47**, 7461–7465.
17 P. Gibot, M. Casas-Cabanas, L. Laffont, S. Levasseur, P. Carlach, S. Hamelet, J. M. Tarascon and C. Masquelier, *Nat. Mater.*, 2008, **7**, 741–747.
18 C. Delacourt, L. Laffont, R. Bouchet, C. Wurm, J. B. Leriche, M. Morcrette, J. M. Tarascon and C. Masquelier, *J. Electrochem. Soc.*, 2005, **152**, A913–A921.
19 A. Yamada, Y. Kudo and K. Y. Liu, *J. Electrochem. Soc.*, 2001, **148**, A1153–A1158.
20 G. Kobayashi, A. Yamada, S. Nishimura, R. Kanno, Y. Kobayashi, S. Seki, Y. Ohno and H. Miyashiro, *J. Power Sources*, 2009, **189**, 397–401.
21 H. L. Wang, Y. Yang, Y. Y. Liang, L. F. Cui, H. S. Casalongue, Y. G. Li, G. S. Hong, Y. Cui and H. J. Dai, *Angew. Chem., Int. Ed.*, 2011, **50**, 7364–7368.
22 C. Delacourt, P. Poizot, J.-M. Tarascon and C. Masquelier, *Nat. Mater.*, 2005, **4**, 254–260.
23 S.-W. Kim, J. Kim, H. Gwon and K. Kang, *J. Electrochem. Soc.*, 2009, **156**, A635–A638.
24 G. Y. Chen and T. J. Richardson, *J. Power Sources*, 2010, **195**, 1221–1224.
25 S. P. Ong, A. Jain, G. Hautier, B. Kang and G. Ceder, *Electrochem. Commun.*, 2010, **12**, 427–430.
26 J. K. Warner, A. K. Cheetham, A. G. Nord, R. B. Vondreele and M. Yethiraj, *J. Mater. Chem.*, 1992, **2**, 191–196.
27 J. P. Perdew, K. Burke and M. Ernzerhof, *Phys. Rev. Lett.*, 1996, **77**, 3865–3868.
28 G. Kresse and J. Furthmuller, *Comput. Mater. Sci.*, 1996, **6**, 15–50.
29 K. Kang, Y. S. Meng, J. Breger, C. P. Grey and G. Ceder, *Science*, 2006, **311**, 977–980.
30 K. Kang, D. Morgan and G. Ceder, *Phys. Rev. B: Condens. Matter Mater. Phys.*, 2009, **79**, 014305.
31 D. H. Seo, H. Gwon, S. W. Kim, J. Kim and K. Kang, *Chem. Mater.*, 2010, **22**, 518–523.
32 F. Zhou, K. S. Kang, T. Maxisch, G. Ceder and D. Morgan, *Solid State Commun.*, 2004, **132**, 181–186.
33 S. W. Martin, *J. Am. Ceram. Soc.*, 1991, **74**, 1767–1784.
34 J. Kim, K.-Y. Park, I.-C. Park, J.-K. Yoo, D.-H. Seo, S.-W. Kim and K. Kang, *J. Electrochem. Soc.*, 2011, **159**, A55–A59.
35 K.-Y. Park and K. Kang, submitted.
36 D. R. Askeland, P. P. Fulay and W. J. Wright, *The Science and Engineering of Materials*, Thomson, 2002.

 